NASA Contractor Report 165471

(NASA-CR-165471) CALCULATIONS OF TRANSONIC POTENTIAL FLOW OVER CASCADES Final Report (Flow Research, Inc., Kent, Wash.) 36 p HC A03/MF A01 CSCL 01A

N82-11041

Unclas G3/02 08252

CALCULATIONS OF TRANSONIC POTENTIAL FLOW OVER CASCADES

Wen-Huei Jou

Flow Research Company
Kent, Washington 98031

October 1981

Prepared for

NATIONAL AERONAUTICS AND SPACE ADMINISTRATION
Lewis Research Center
Under Contract NAS3-22129

Table of Contents

1. Introduction

Recent advances in the computation of transonic potential flows around airfoils and around complex aircraft have provided powerful tools for the aerodynamic design of an aircraft (Caughey and Jameson, 1979; Mercer and Murman, 1980). These computational codes are used extensively in practical aircraft designing to the extent that the entire aerodynamic configuration can be determined by using computational techniques (Jupp, 1980). These advances can also be readily applied to the flow around a rotor in turbomachinery.

The applicability of the steady potential flow assumption to flow around a rotor has been discussed in the past (Jou, 1979; Dulikravich, 1979). The main conclusion is that in a rotating fixed-blade frame of reference, a reduced potential exists such that its gradient is the perturbation velocity. Both Dulikravich (1979) and Adamczyk (1980) have applied the finite volume technique to flows around cascades, and Dulikravich has extended the computations to three-dimensional flows. The features of these two works are listed in the following table.

	Dulikravich	Adamczyk
Mesh	O-type: Conformal mapping and shearing	O-type: Generated by an electrostatic problem
Full Potential	Yes	Yes
Conservative	Yes	Yes
Artificial Dissipation	Artificial Viscosity	Artificial Density
Solution Algorithm	SLOR	SLOR
Dimensions	Two and Three	Two

There are a few questions remaining to be answered. Due to geometrical constraints, the O-type mesh cannot sufficiently track a vortex wake far downstream. Whether the induced flow is accurately computed in the three-dimensional case remains to be verified. A C-type mesh seems to be more desirable in the three-dimensional computations. The different methods of implementing the artificial dissipation in the artificial viscosity formulation and the artificial density formulation (Hafez et al., 1978) need a fair comparison in their merits. This can be achieved only by using a code with exactly the same algorithm except for the dissipation terms. The last and one of the most important questions is whether an algorithm more efficient than the successive line overrelaxation scheme can be developed. An efficient algorithm is an important element in using the numerical method for design purposes.

The present work focuses on the following aspects of the finite volume calculation:

(1) Development of a two-dimensional finite volume SLOR code using a C-type mesh coordinate system.

(2) Development of a scheme with both the artificial viscosity and artificial density options and comparison of the results of the computation.

(3) Investigation of possible means to accelerate the convergence of the computation.

(4) Recommendations for the development of a three-dimensional code based on the two-dimensional investigation.

Dr. John Adamczyk has provided the original mesh generation scheme PJGRID for modification in this work.

2. Finite Volume Method, Artificial Density Formulation, and Nonlinear Iteration

The finite volume method has been reported in detail by Jameson and Caughey (1977) and does not require an extensive review here. However, there is some confusion about (1) whether the method is a finite difference or finite element method, (2) how the nonlinear term is linearized during the iteration, and (3) how an artificial density concept would be implemented. The present section intends to clarify these questions.

The finite volume scheme as implemented by Jameson and Caughey (1977) consists of the following procedure:

(a) Mapping of the physical domain into a rectangular computational domain (construction of curvilinear coordinates).

(b) Computing the flux $\rho h U^i$ at the center of the cell formed by coordinate lines as shown in Figure 1. The flux is computed using the local bilinear variation of the potential $\phi(x_i)$ and the transformation $x_i(x_j)$.

(c) Adding a recoupling term which effectively relocates the point of evaluated flux $\rho h U$ a distance δ away from the center as shown in Figure 1. Here, $\delta \leq 1/2$. (In the present version, the variation of h has not been included.)

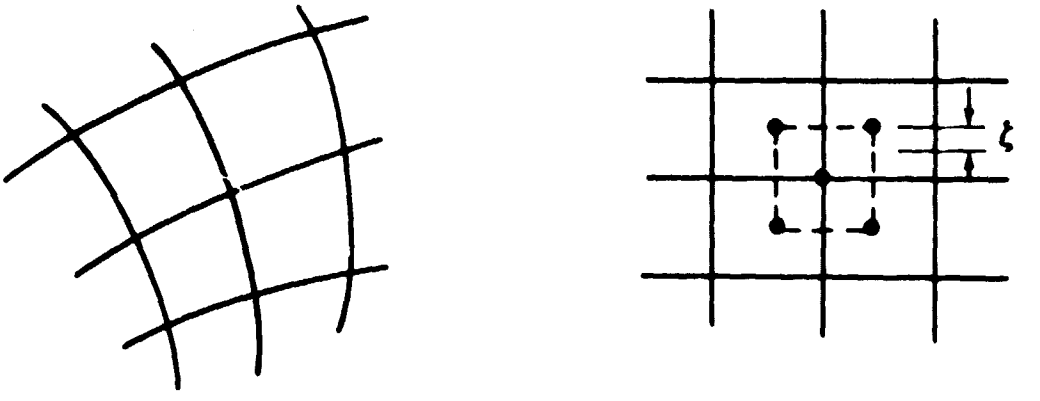

Figure 1. Local Coordinate Transformation

(d) Forming the flux balance for the "secondary" cell represented by the dotted line in Figure 1.

(e) Adding the artificial time-dependent term.

(f) Adding the artificial viscosity term.

To see the relation between the above procedure and the finite element method, one should start with the Bateman variation principle; i.e., conservation of mass can be recovered if the variation of the following integral is carried out:

$$I = \int p \, d\Omega \tag{1}$$

where

$$p = \rho^{\gamma} \tag{2}$$

and

$$\rho = \left[1 + \frac{\gamma-1}{2} M_{\infty}^2 (1 - \nabla\phi \cdot \nabla\phi)\right]^{\frac{1}{\gamma-1}} . \tag{3}$$

By transforming the domain of integration from the physical space $\Omega(\vec{x})$ to the computational space $\overline{\Omega}(\vec{X})$, the integral becomes

$$I = \int \rho h \, d\overline{\Omega} \tag{4}$$

with

$$\rho = \left[1 + \frac{\gamma-1}{2} M_{\infty}^2 (1 - U^i \frac{\partial \phi}{\partial X^i})\right]^{\frac{1}{\gamma-1}} . \tag{5}$$

The finite element method amounts to approximating I by a sum of integrals over small discretized elements:

$$I = \sum_{n=1}^{N} \int_{F.E.} \rho h \, d\overline{\Omega} . \tag{6}$$

To evaluate the integral inside the elements, certain trial functions for ϕ and $x_i(X_j)$ must be assumed. If bilinear dependence of ϕ on X_j is chosen for the elements, these integrals can be evaluated explicitly in terms of the values of ϕ at the corners of the elements. The variation of the integral with respect to these corner values gives the discretized system of equations for ϕ. It can be shown by fairly tedius calculations that if the integral in the element is evaluated by expanding the integrand in a Taylor series

around the center of the element, the variational procedure leads to a discretized problem corresponding to the finite volume method with the displacement factor $\delta = 1/6$. Aside from the artificial time-dependent term and the artificial viscosity term, the finite volume method is indeed an approximation to the finite element method. However, the artificial viscosity term requires evaluations of the higher order derivatives (ϕ_{XX} , etc.) within the element. Hence, with the bilinear element, there is no way that the information of artificial viscosity can be contained inside the element. Up to now this term has been treated in the finite difference manner in all the existing finite element works (e.g., Deconinck and Hirsch, 1980). It is also the root of the problem in using more flexible triangular-type finite element calculations.

The artificial density version of the dissipation in transonic computations (Hafez et al., 1978) has gained some popularity. In an arbitrary mesh, the following derivation gives the proper form of the artificial density:

$$\bar{\rho} = \rho - \mu \rho_s \Delta s \tag{7}$$

$$\rho_s = \frac{1}{h^{1/2} q} \left[U\rho_X + V\rho_Y \right] \tag{8}$$

$$\left|\left| \Delta s \right|\right| = \left|\left| \frac{1}{h^{1/2} q} (UV) \begin{pmatrix} \frac{\partial x}{\partial X} & \frac{\partial x}{\partial Y} \\ \frac{\partial y}{\partial X} & \frac{\partial y}{\partial Y} \end{pmatrix} \right|\right| \tag{9}$$

or

$$\left|\left| \Delta s \right|\right| = \frac{1}{h^{1/2} q} \left|\left| \begin{pmatrix} U \frac{\partial x}{\partial X} + V \frac{\partial y}{\partial X} \\ U \frac{\partial x}{\partial Y} + V \frac{\partial y}{\partial Y} \end{pmatrix} \right|\right| \tag{10}$$

$$= \frac{1}{h^{1/2} q} \left|\left| \begin{pmatrix} C_X \\ C_Y \end{pmatrix} \right|\right|$$

where (C_X, C_Y) are the covariant components of the velocity vector. Letting the norm of the vector (C_X, C_Y) be defined as $(|C_X| + |C_Y|)$, we have

$$\rho_s \Delta s \simeq \frac{1}{hq^2} (|C_X| + |C_Y|) (U\rho_X + V\rho_Y) \quad . \tag{11}$$

This expression avoids taking the square root in the computation. The derivatives ρ_x and ρ_y are evaluated in the upwind direction, while the switching function μ is evaluated one-half mesh upwind.

The use of artificial density is usually coupled with an iterative procedure different from that used in the artificial viscosity version. In the fully implicit iteration procedure of the artificial viscosity version originally formulated by Jameson, the nonlinearity of the governing equation is linearized in the following manner:

$$\nabla\cdot(\rho^{n+1}\nabla\phi^{n+1}) = 0 \tag{12}$$

$$\phi^{n+1} = \phi^{n} + C \tag{13}$$

$$\rho^{n+1} = \rho^{n} + \nabla_{\vec{V}}\rho^{n}\cdot\nabla C \tag{14}$$

where C is the correction to the velocity potential and $\nabla_{\vec{V}}$ is the gradient in the velocity space. Hence, the equation for the correction C is

$$\nabla\cdot\left(\rho^{n}\nabla C + (\nabla_{\vec{V}}\rho^{n}\cdot\nabla C)\nabla\phi^{n}\right) = -\nabla\cdot(\rho^{n}\nabla\phi^{n}) \quad . \tag{15}$$

Although Jameson does not take full account of the left-hand side, he does include the factors $[(1 - u^2/a^2)$, etc.], which appear in the quasi-linear version of the governing equation. The iteration is, although not to the full extent, an implicit method. The iteration procedure which is often used in conjunction with the artificial density version is

$$\nabla\cdot(\bar{\rho}^{n}\nabla\phi^{n+1}) = 0 \quad . \tag{16}$$

The artificial density $\bar{\rho}$ is evaluated from the last iteration. The The procedure is semiimplicit. This explicit use of $\bar{\rho}$ caused Hafez (1979) to call it an "elliptic" method. The use of the terminology is unfortunately not justified. The mathematical nature of the equation can only be defined by discussing the equivalent time-dependent problem in which the steady-state problem is embedded.

To illuminate this, we consider a simpler model equation (small disturbance):

$$\begin{cases} (\rho\phi_x)_x + \phi_{yy} = 0 \\ \rho = 1 - \dfrac{\phi_x}{2} \end{cases} \tag{17}$$

Now,

$$\begin{aligned} \rho^n &= \rho^{n+1} - \rho_t^{n+1}\Delta t \\ &= \rho^{n+1} + \phi_{xt}^{n+1}\frac{\Delta t}{2} \end{aligned} \tag{18}$$

By substituting these relations into the governing equation with a semiimplicit iteration procedure, one produces the following time-dependent problem:

$$(\rho\phi_x)_x + \phi_{yy} + \frac{\Delta t}{2}(\phi_{xt}\phi_x)_x = 0 \tag{19}$$

$$(1 - \phi_x + \frac{\Delta t}{2}\phi_{xt})\phi_{xx} + \phi_{yy} + (\frac{\Delta t}{2}\phi_x)\phi_{xxt} = 0 \quad . \tag{20}$$

Since all variables are in the $(n + 1)$ level, the superscripts are omitted. There is an additional artificial time-dependent term ϕ_{xt} which is added to enhance the stability (Jameson, 1974). The complete time-dependent problem with the artificial dissipation can be represented by the following equation:

$$-\alpha\phi_{xt} + A\phi_{xx} + \phi_{yy} + \mu\phi_{xxx} + \varepsilon\phi_{xxt} = 0 \tag{21}$$

where α, A, μ, and ε are functions of the solution ϕ itself. It should be remembered that $\mu = O(\Delta x)$ and $\varepsilon = O(\Delta t)$. The third-order terms are of singular perturbation type. The effects of the additional term ϕ_{xxt} to the unsteady solution remain to be studied. It cannot be pronounced simply as an elliptic problem in the spatial domain.

3. Numerical Code

The numerical code developed here is based on the two-dimensional finite volume code, FLO 26, developed by Jameson for flow around an airfoil. The modifications include: (1) generation of a C-type grid for cascades, (2) the boundary conditions on both the periodic boundaries and the upstream and downstream boundaries, and (3) the artificial density option in the solver. These are discussed in the following subsections.

3.1 Mesh Generation

The mesh generation routine in the present work is the modification of an O-type mesh generator by Adamczyk (1980). The method is based on an electrostatic problem of a cascade charged with V = 1 and V = -1 on alternate blades. The equipotential lines and the flux lines are used as the coordinate lines. To adopt the method for generating a C-type mesh to be used in a finite volume calculation, the following modifications are made to the original mesh generation routine:

(1) A straight line is attached to the trailing edge of the blade. This straight line is an approximation of the trajectory of the vortex wake (in the three-dimensional case) and is assumed to be at the angle of the bisecting line of the trailing edge. The blade and the straight line are charged with the same potential in the electrostatic problem.

(2) The resulting O-type mesh system around the combined geometry of blade and wake is truncated near the downstream end of the straight line (the wake). The resulting mesh is of the C type as far as the original blade system is concerned.

(3) To ensure that a mesh line will pass through the trailing edge, a shearing transformation is applied. This shearing

transformation also adjusts the number of meshes on the blade to a multiple of four. The purpose is to perform computations on successively refined meshes to increase the rate of convergence.

(4) The mesh lines intersecting the "wake" are sheared so that they are continuous across the wake.

Other improvements on the mesh generation scheme are also performed. Most importantly, the input data of blade geometry is interpolated into a more coarsely spaced approximate blade shape. An approximate mesh system is generated. The mesh lines are then sheared to the exact blade position. This procedure increases the speed of the mesh generation procedure without loss of accuracy in defining the blade geometry. The results of the mesh generation are shown in Figures 2, 4, and 9.

3.2 Boundary Conditions

On the periodic line, an extended computational domain is established by including the next "exterior" mesh lines, as shown by the dotted lines in Figure 3. The values of the potential on these "exterior lines" are given by the previous iteration from the condition of periodicity. These values are used as the Dirichlet boundary conditions.

On the exit boundary, the boundary condition that the flow field attains its asymptotic downstream state is imposed. After each iteration, the circulation around the blade Γ is computed. The far-field conditions are computed by the solution of the following equations:

$$\cos \alpha_1 = \rho_2 q_2 \cos \alpha_2 \tag{22}$$

$$\sin \alpha_1 = q_2 \sin \alpha_2 + \frac{\Gamma}{H} \tag{23}$$

$$\rho_2 = \left[1 + \frac{\gamma-1}{2} M_\infty^2 (1 - q_2^2)\right]^{\frac{1}{\gamma-1}} \tag{24}$$

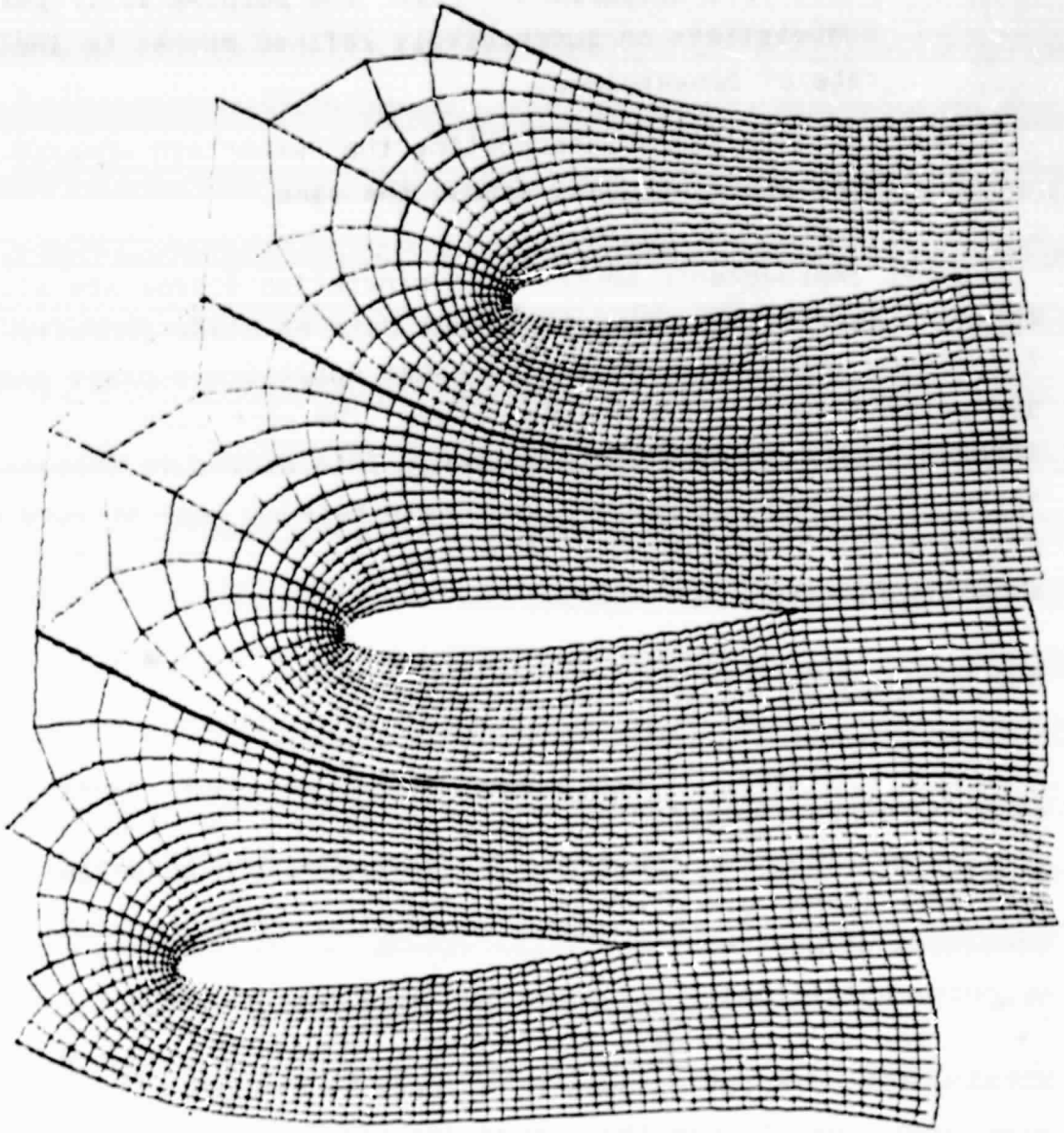

Figure 2. Fine Grid for NACA 0012

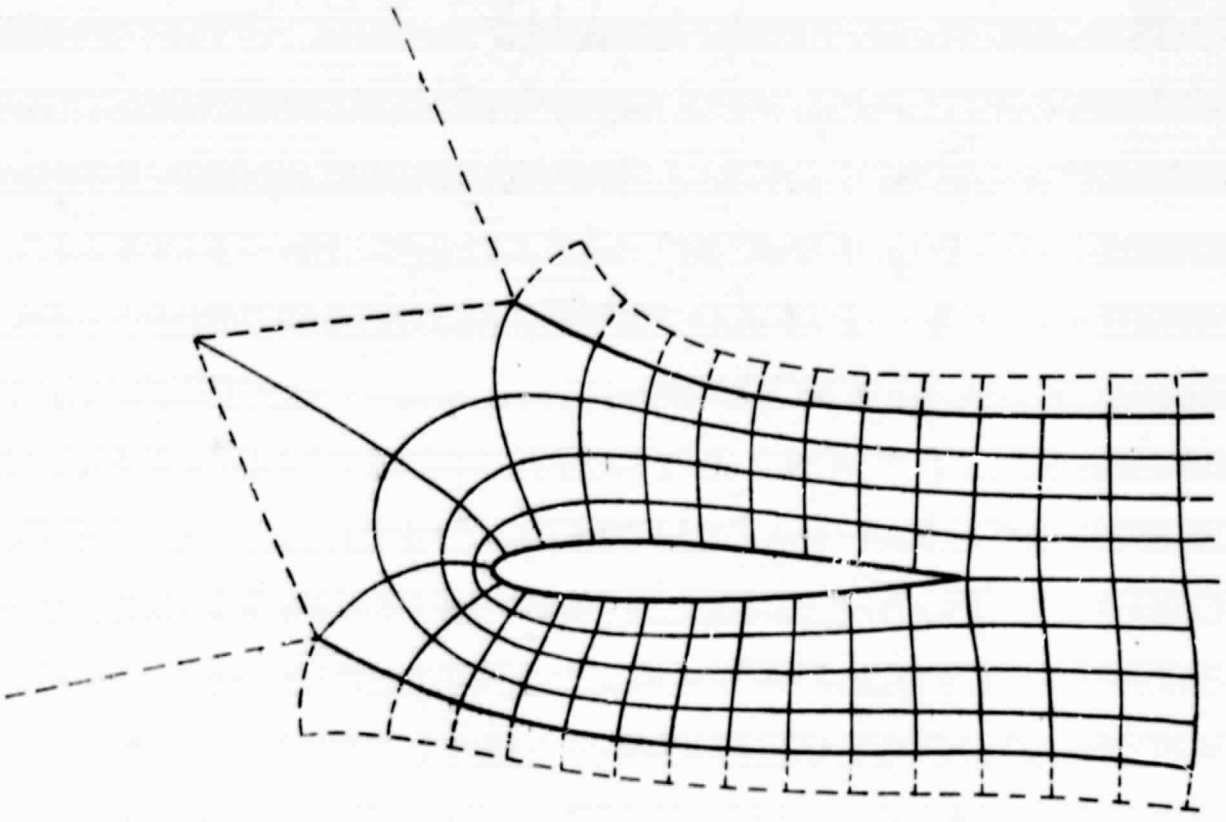

Figure 3. Computational Domain and Boundary Conditions

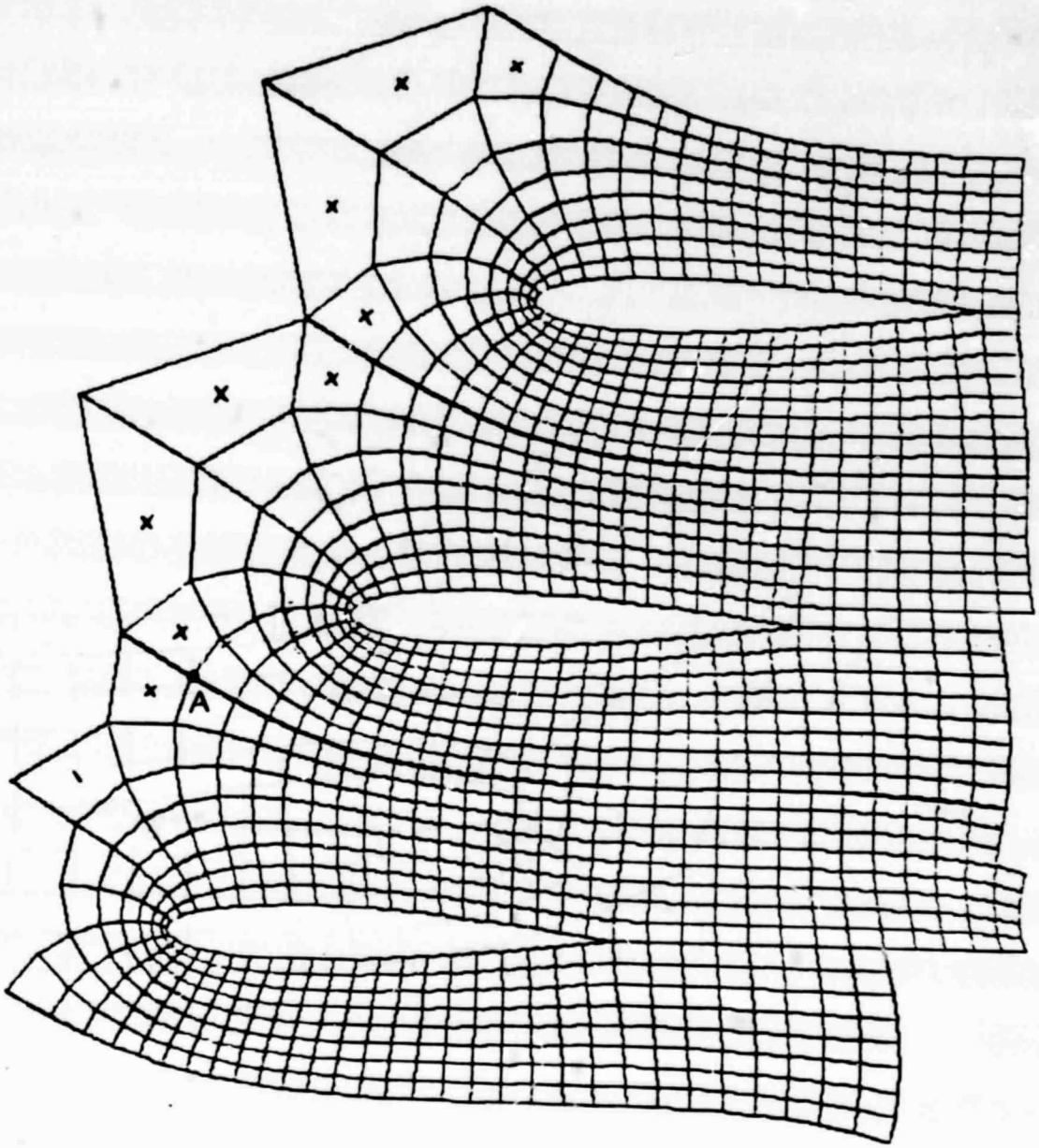

NACA 0012
STAGGER ANGLE 30.00
PITCH .794
CASCADE GRID 64 X 8

Figure 4. Medium Grid for NACA 0012

where α_1 and α_2 are the flow angles far upstream and downstream, respectively; ρ_2 and q_2 are the density and the speed far downstream; and H is the pitch distance. Using the farfield velocity vector (q_2, α_2), the values of the velocity potential on the boundary points are obtained by integration from the neighboring interior points. These potential values are used as Dirichlet conditions for the next iteration.

As for the inflow boundary, we choose to use the Neumann boundary condition. Referring to Figure 4, the physical velocity components (u, v) at the center of the inflow boundary cells, marked with the cross, are given by the prescribed upstream condition. Contravariant velocities are computed from the given velocity for flux balance.

These boundary conditions are implemented numerically and they have proven to produce a stable iteration procedure.

3.3 Artificial Density Option

The artificial density formulation, with an explicit evaluation of the artificial density from the previous iteration as discussed in Section 2, is coded as an option in the solver subroutine. With this option, the merits of one against the other can easily be evaluated. Further discussions will be given in Section 4.

4. Numerical Results and Discussion

Two blade geometries are chosen for developing the numerical code. The NACA 0012 configuration is chosen for comparing the results to the single airfoil calculations so that the effects of a cascade can be seen. Sanz's shock-free compressor blade is chosen to validate the code against the design conditions.

Figures 5 and 6 show the computed pressure distribution on the NACA 0012 with a pitch distance of 1.98 C at Mach number 0.75 ($M_\infty = 0.75$) with an angle of attack relative to the blades at -2 degrees ($\alpha = -2^\circ$) and at various stagger angles. The effects of a cascade are obvious from a comparison of these figures. These results have been obtained by using the artificial viscosity version. Figure 7 shows the results of computation using the artificial density version with the same artificial dissipation coefficient as that used in the artificial viscosity version. There are ripples ahead of the shock wave and the solution is slowly diverging. With the increase of the dissipation coefficient to 1.8 times that previously used, the solution converges; the results are shown in Figure 8. The convergence rate, as well as the quality of the shock resolution, is comparable for these two types of formulations for artificial dissipation.

For Sanz's shock-free blade, the preliminary calculations using the given data show unreasonable results near the leading edge. A close examination of the blade data reveals a lack of data points near the crucial leading-edge region. The data around that region are filled in by visual interpolations. Figure 10 shows the results of computations for the design condition. The results compare very well with the Mach number distribution for the design condition. These results are computed using the artificial density version. The computations of the same case using the artificial viscosity version with a coefficient of dissipation as large as 3 are shown in Figure 11. Notice the bad results near the leading edge. Experiences in the past have shown that the artificial viscosity version

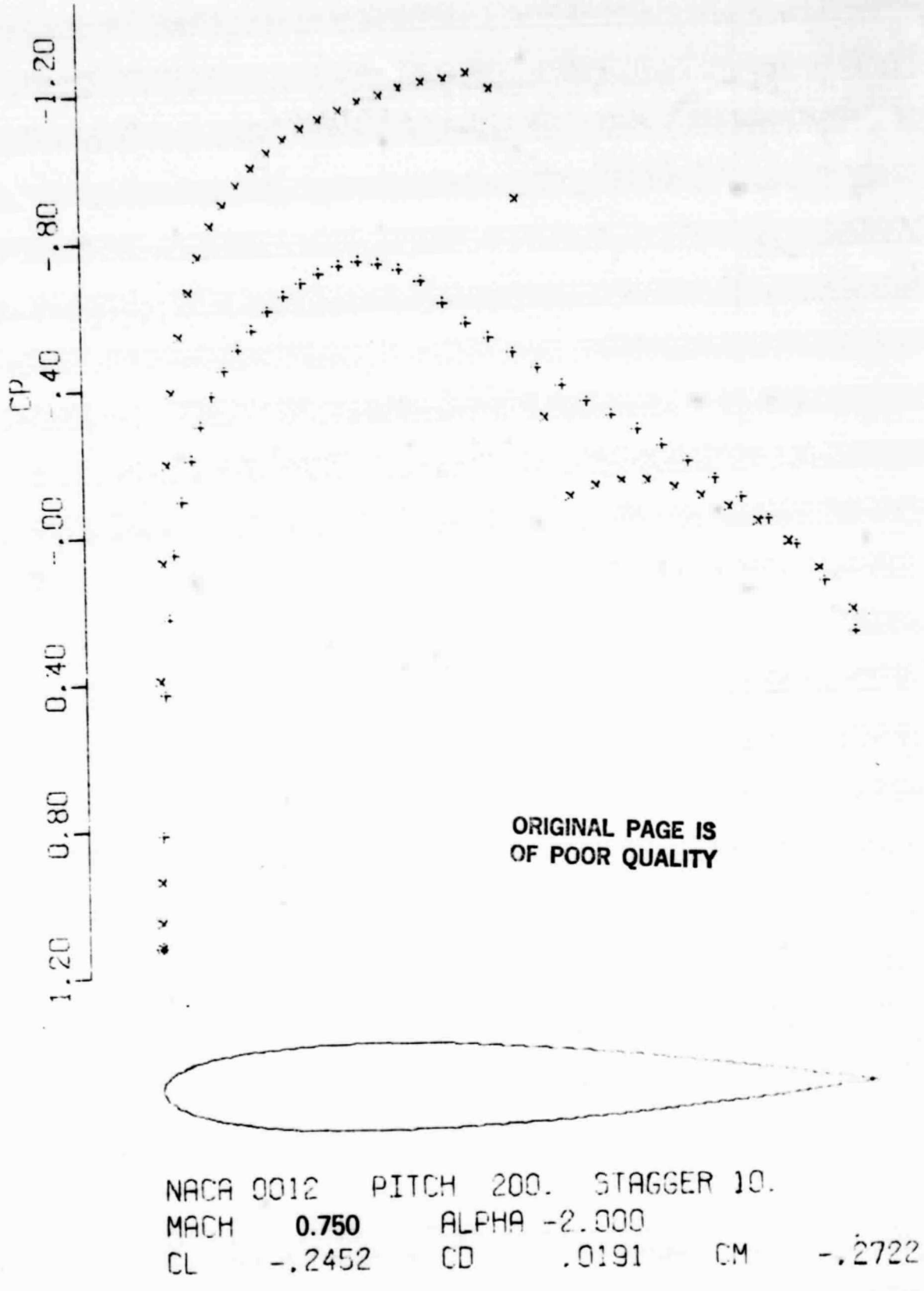

Figure 5. Pressure Distribution (NACA 0012) (I)
(For NACA0012 ALPHA Is Relative to the Chord)

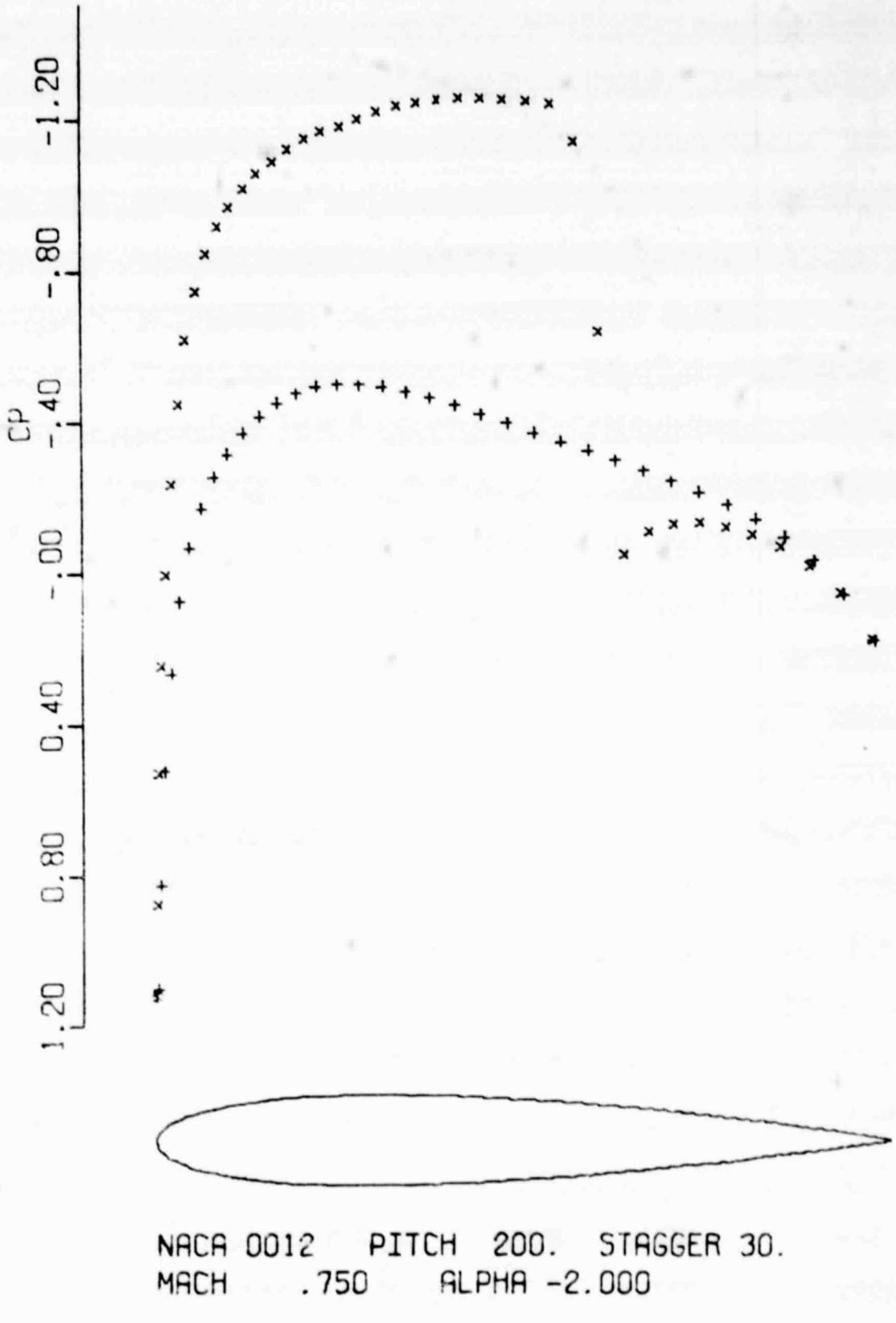

Figure 6. Pressure Distribution (NACA 0012) (2)

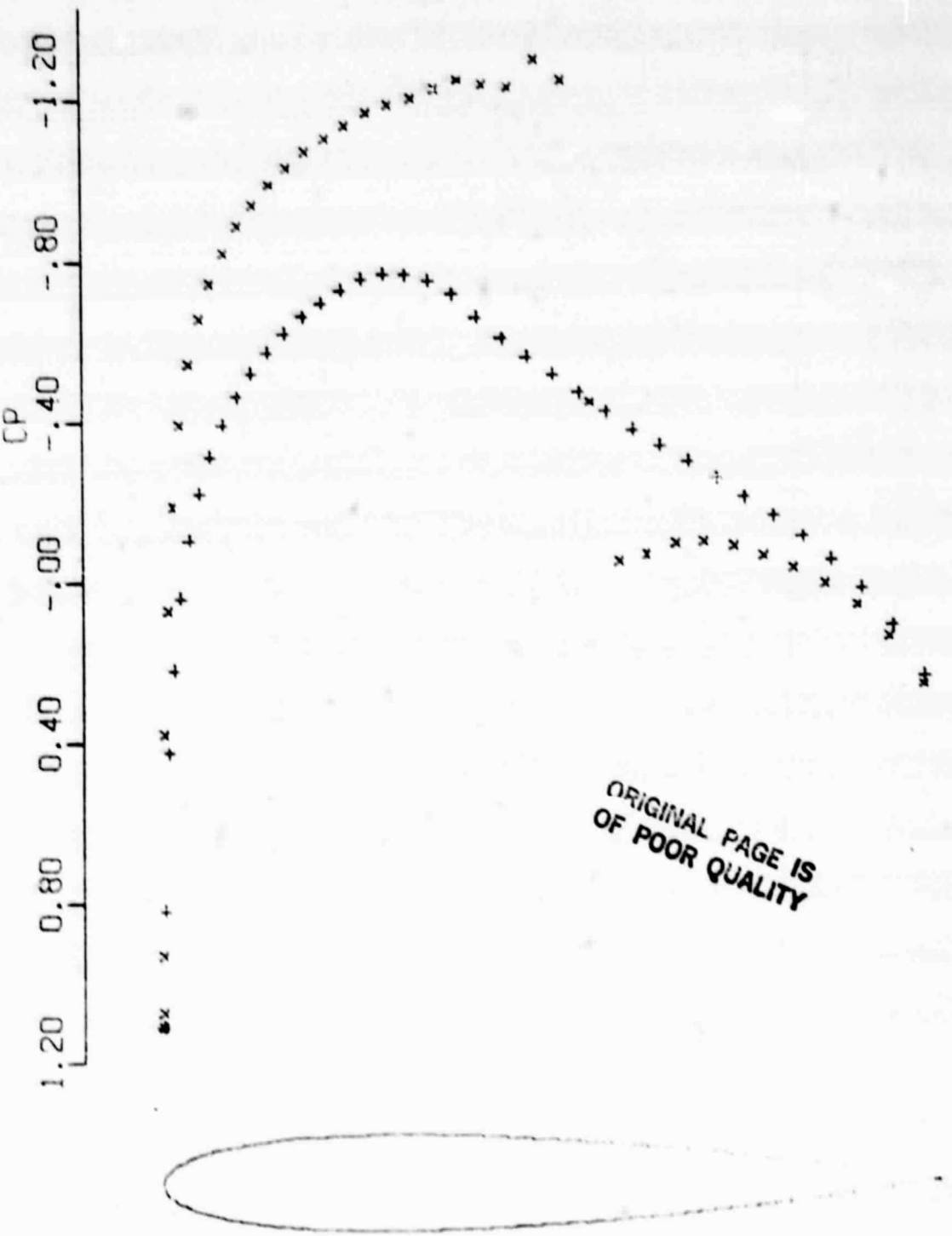

Figure 7. Calculation Using Artificial Density
$\bar{\varrho} = \varrho - \mu \varrho_s \Delta s$; $\mu = \text{Max}[(1 - \frac{1}{M^2}), 0]$

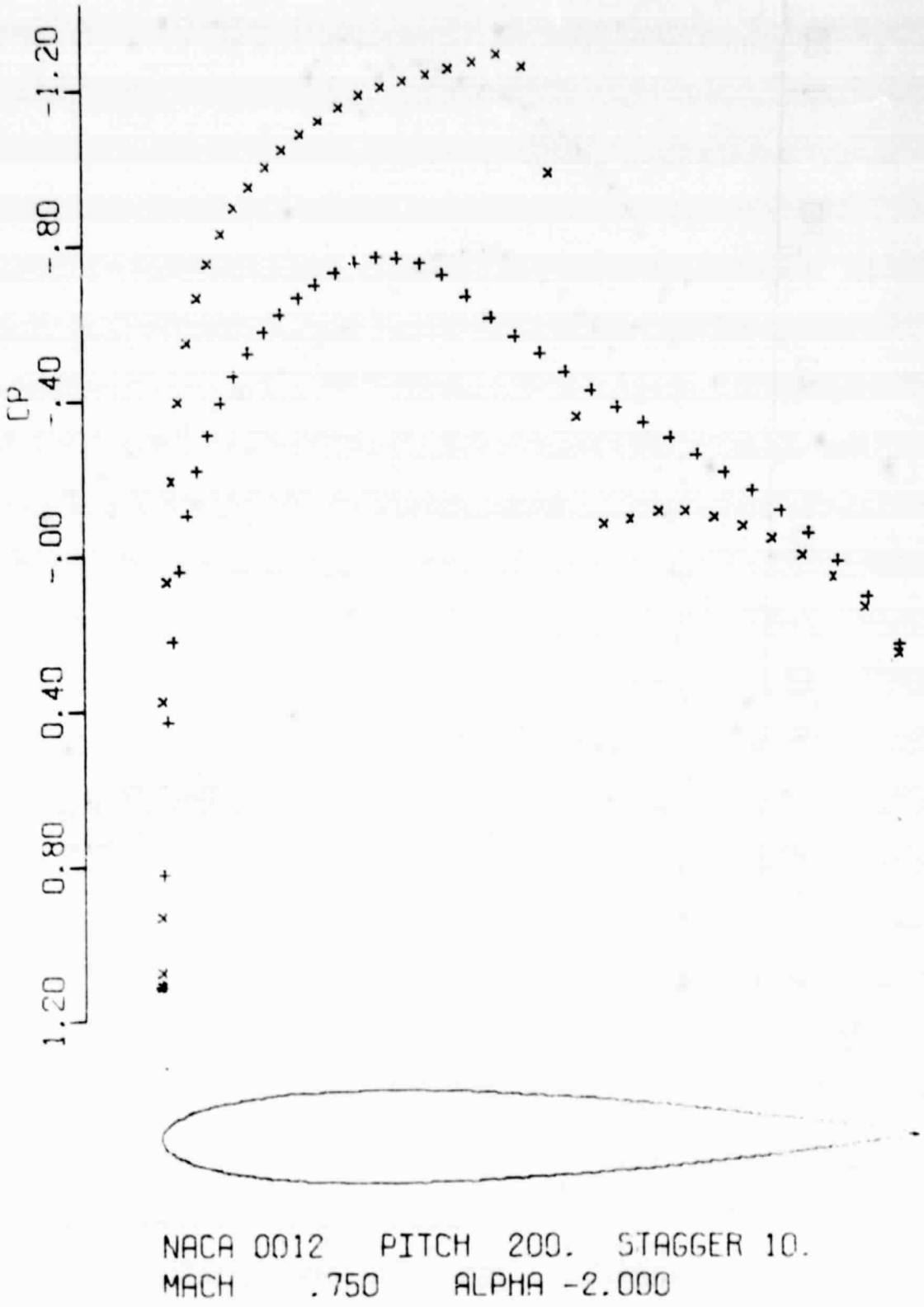

Figure 8. Calculation Using Artificial Density
$\bar{\varrho} = \varrho - \mu \varrho_s \Delta s \; ; \; \mu = \text{Max}\left[1.8\left(1 - \frac{1}{M^2}\right), 0\right]$

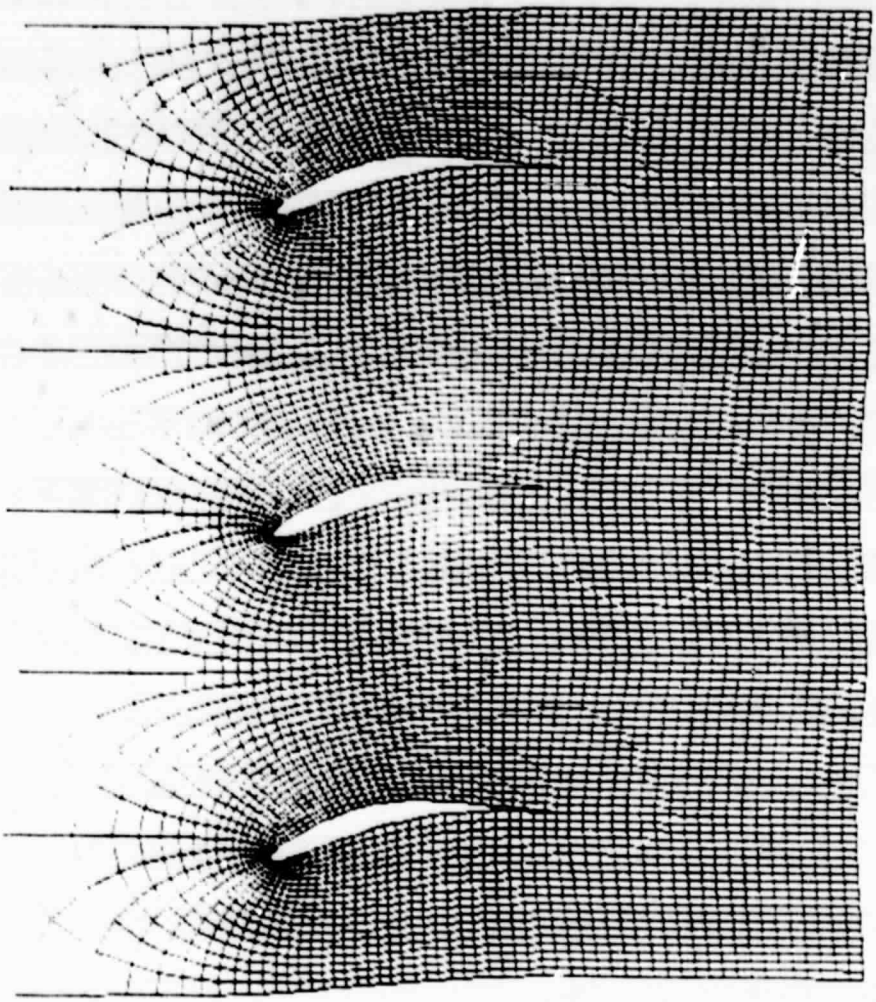

Figure 9. Fine Grid for Sanz Blade

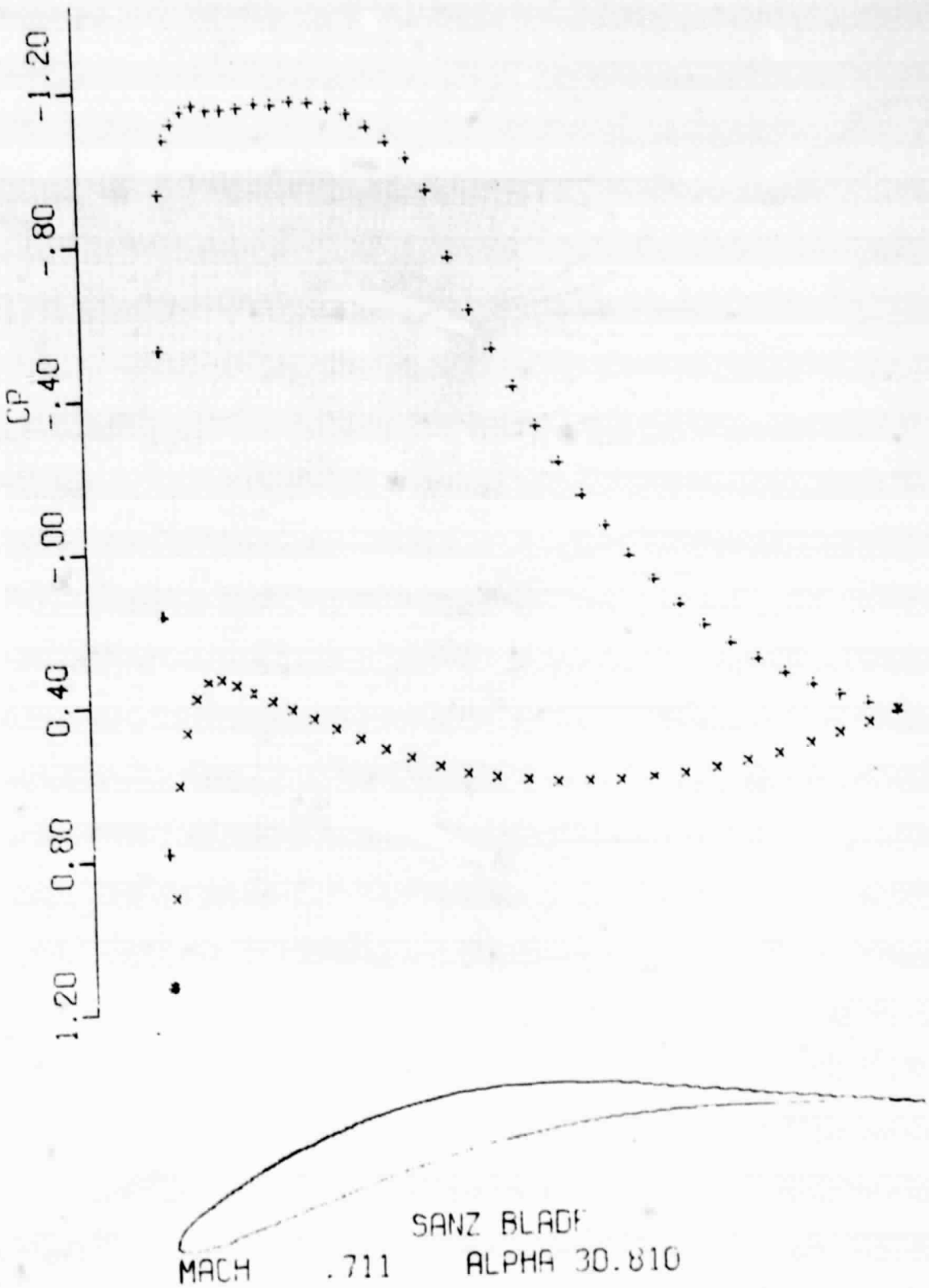

Figure 10. Pressure Distribution at Design Condition (Sanz Blade) (ALPHA Relative to Horizontal Direction)

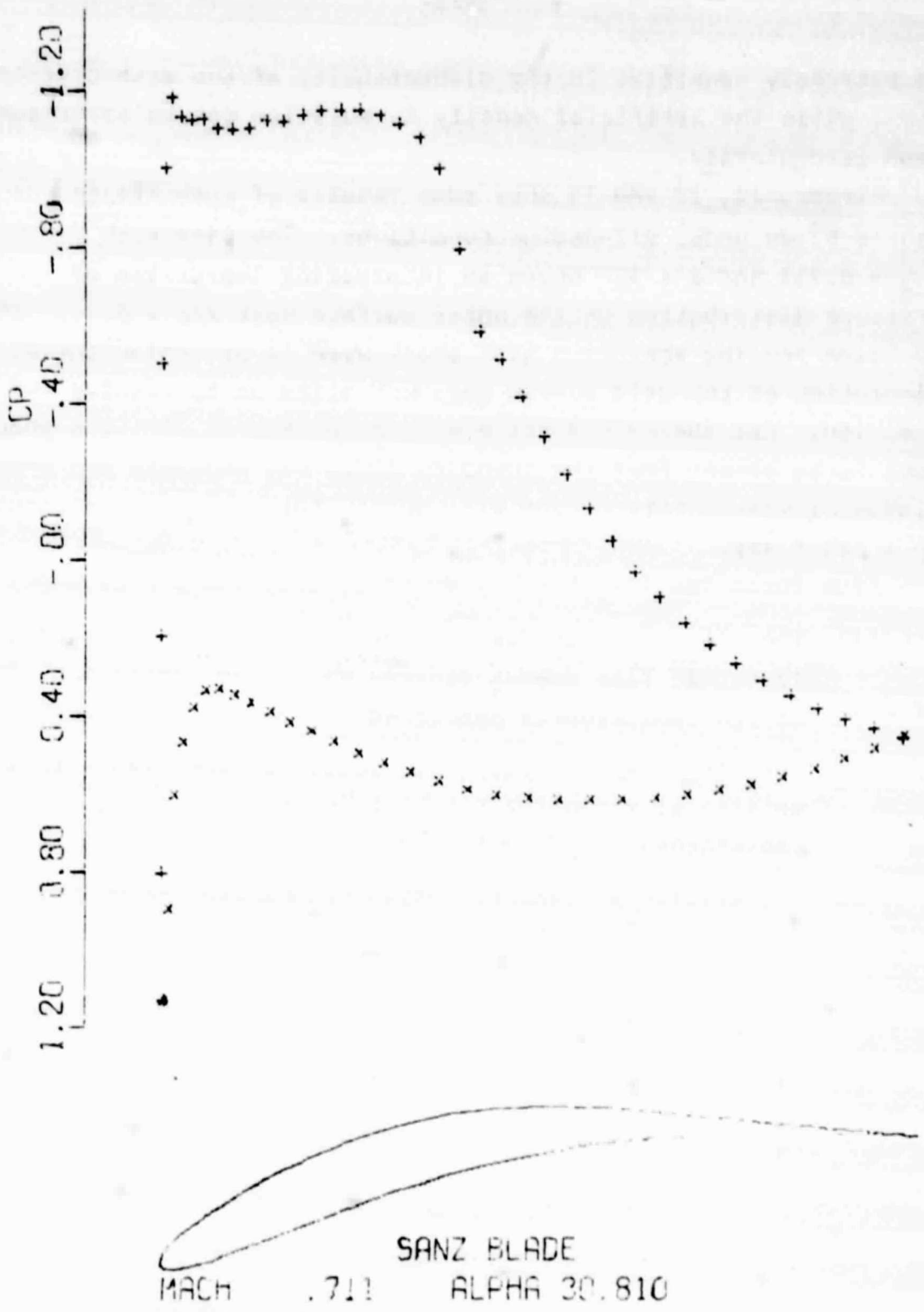

Figure 11. Pressure Distribution Using Artificial Viscosity

is extremely sensitive to the discontinuity of the mesh distribution, while the artificial density formulation can tolerate some mesh irregularity.

Figures 12, 13 and 14 show some results of computations of Sanz's blade under off-design conditions. The case with $M_{-\infty} = 0.711$ and $\alpha = 32°$ shows an interesting depression of pressure distribution on the upper surface near $x/c = 0.28$. The question remains whether a weak shock wave is presented there. The resolution of the grid system does not allow us to resolve the question. For the case where $M = 0.78$ and $\alpha = 30.81°$, the shock wave is so strong that the boundary layer may separate and a strong viscous-inviscid interaction will modify the pressure distribution in a major way.

From these results, the following conclusions can be made:

(1) The analysis code does produce an accurate solution of the transonic flow over a cascade as far as comparison with the design condition is concerned.

(2) The artificial density formulation is comparable to the artificial viscosity formulation in both accuracy and convergence.

(3) The artificial density option can handle the mesh discontinuity better than the artificial viscosity version.

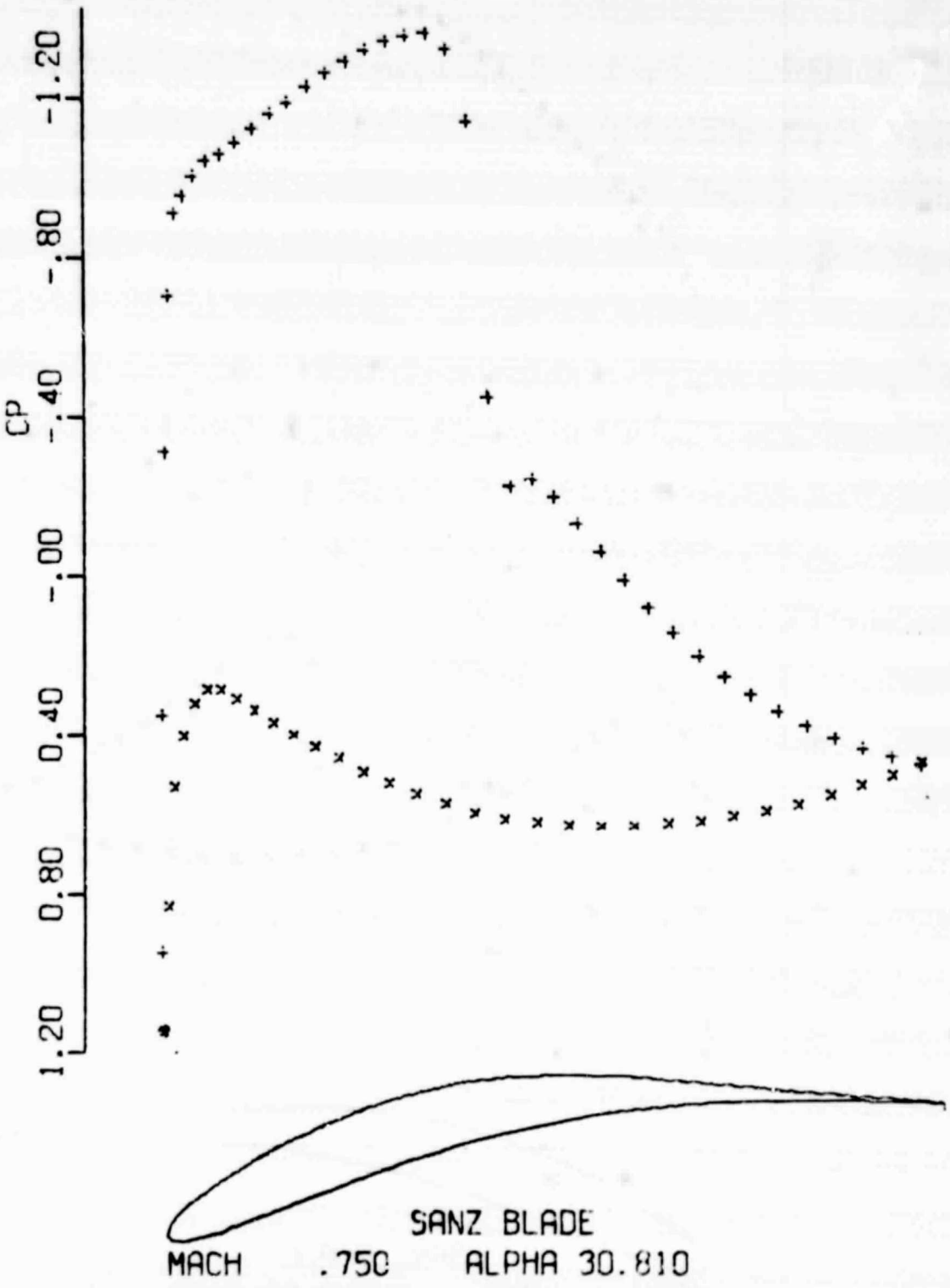

Figure 12. Pressure Distribution at Off-Design Condition (1)

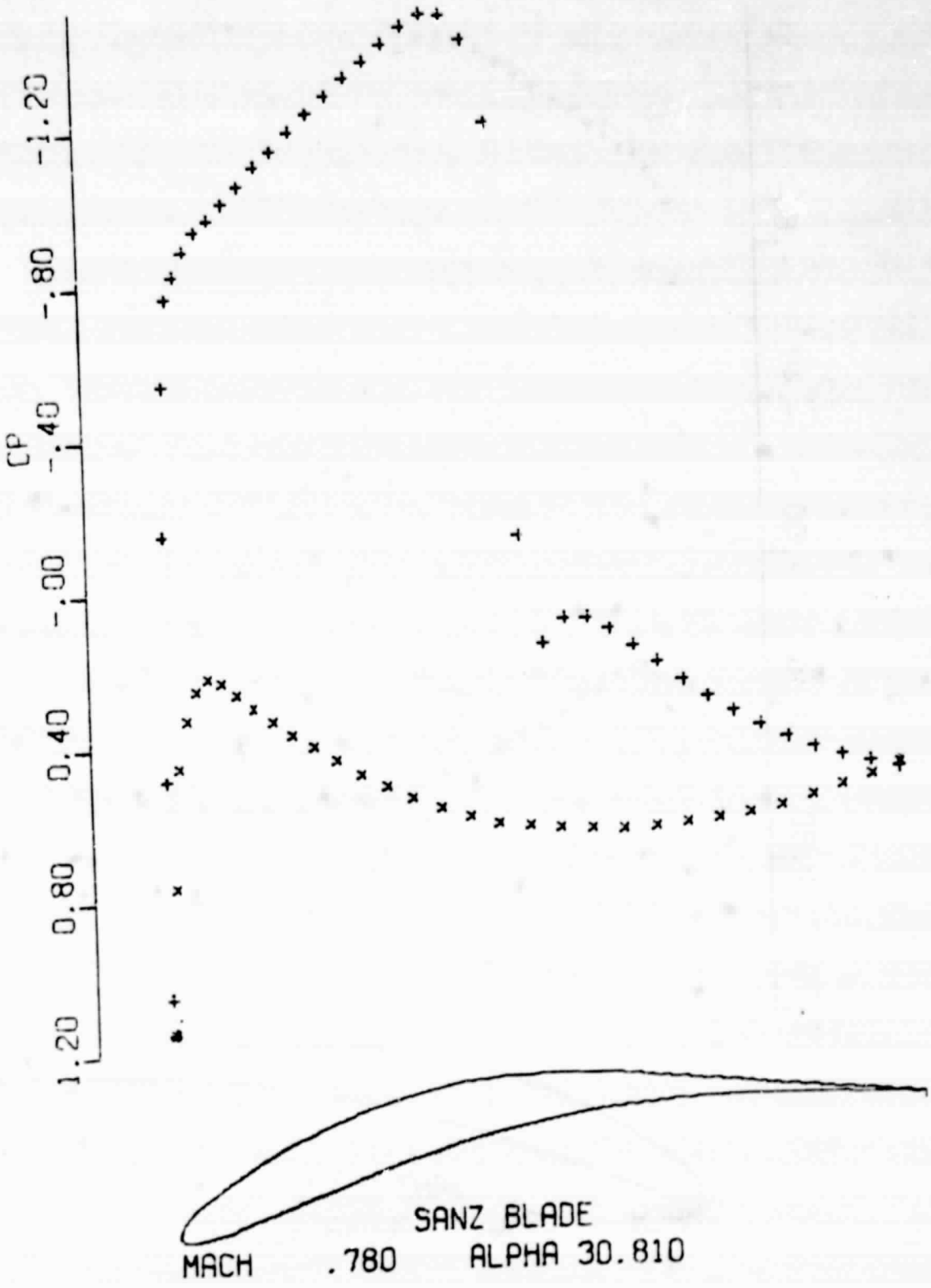

Figure 13. Pressure Distribution at Off-Design Condition (2)

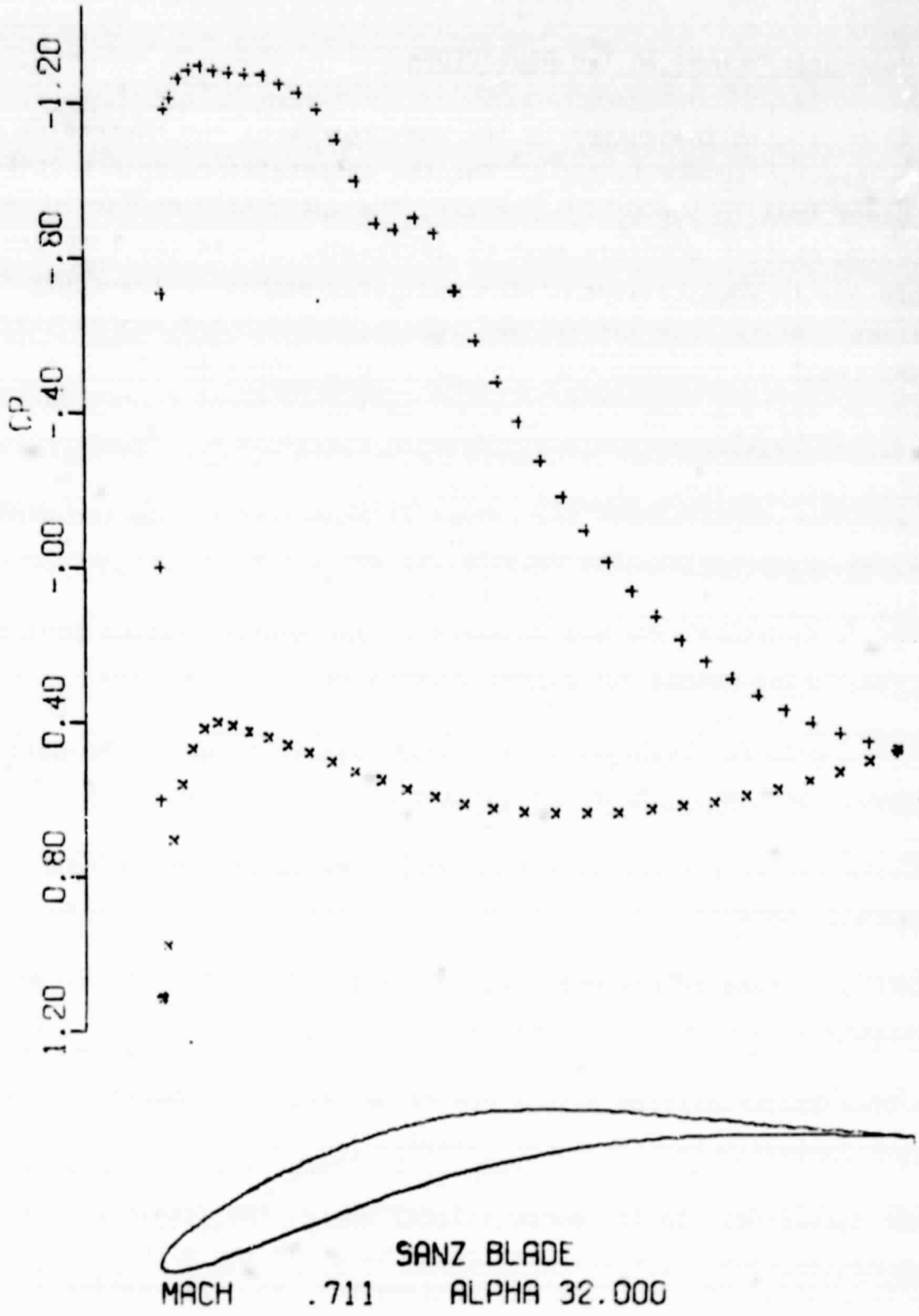

Figure 14. Pressure Distribution at Off-Design Condition (3)

5. Multigrid Method in Two Dimensions

As mentioned in Section 1, the convergence of the successive line overrelaxation scheme is slow. For the computational method to be an efficient tool in the design process, the speed of computation in achieving certain accuracy must be increased. There are some recent progresses in applications of the multigrid method to transonic flow problems. Aside from the earlier report of South and Brandt (1977) on the small disturbance equation, Arlinger (1980) has reported successes in applications of the method to multielement configurations as well as axisymmetric flows. Jameson (1979) in his recent work has coupled the ADI scheme with the multigrid method and has shown some spectacular reductions in the effort of computation. In the present work, we shall explore the possibility and the method of applying the multigrid method to the cascade problem.

It is believed that the successive line overrelaxation scheme is a poor smoothing scheme for high-frequency components of the error in the multigrid computation. The blame is not on the relaxation process itself but on the stretching of the coordinate lines in the airfoil problem. It can be shown that if the mesh size Δx in the marching direction is small compared to Δy in the line direction, the amplification factor for the iteration procedure approaches unity for high-frequency components as $\Delta x/\Delta y$ approaches zero (South and Brandt, 1977). Thus, Jameson (1979) was forced to use the ADI scheme as the smoothing scheme in his multigrid process. The situation is quite different in the cascade problem. The mesh size in the line direction is restricted by the gap distance and requires no stretching at all. The line overrelaxation method can be an effective smoothing scheme in the multigrid process. Furthermore, the number of meshes across the gap is usually limited, while it is quite a large number in the other direction. In the computational space, the domain of interest is a narrow band. The information exchange in the direction of the gap is achieved by the line relaxation; but, the information is propagated one mesh per iteration in the direction of the passage. It is particularly desirable to use the idea of the multigrid in the

direction of the passage, i.e., the longer dimension in the computational domain. To test the idea, a preliminary effort in that direction has been performed in the present work.

Following Jameson (1979), the following multigrid scheme is formulated. For the nonlinear equation $L_h(\phi) = 0$, the finegrid approximation ϕ_h is obtained by the smoothing scheme. The residue in the fine grid R_h is obtained. The correction in the coarser mesh can be obtained as

$$L_{2h}(G_{2h}) = -I_h^{2h}(R_h) \quad , \tag{25}$$

where I_h^{2h} is an interpolation operator from the fine grid to the coarse grid which will filter out the high-frequency component of the residue. But, L_{2h} is a nonlinear operator depending on the coarse mesh potential ϕ_{2h}. To use the same nonlinear smoothing scheme (SLOR) in the same form as that in the fine mesh, we add $L_{2h}(\phi_h)$ to both sides of the coarse-mesh correction equation to form

$$\begin{aligned} L_{2h}(\phi_h + G_{2h}) &= L_{2h}(\phi_{2h}) \\ &= L_{2h}(\phi_h) - I_h^{2h}(R_h) \quad . \end{aligned} \tag{26}$$

So, after the fine-grid solution ϕ_h is obtained, the right-hand side of the above equation is evaluated. The smoothing scheme (SLOR) is again used to obtain ϕ_{2h} . To correct the fine-mesh solution, the reverse operation is applied; i.e.,

$$G_{2h} = \phi_{2h} - \left[\phi_h\right]_{\text{at } 2h \text{ mesh}} \tag{27}$$

$$\phi_h^{n+1} = \phi_h^n + I_{2h}^h(G_{2h}) \tag{28}$$

where n denotes the level of iteration and I_{2h}^h is the interpolation operator which interpolates the correction from the coarse grid G_{2h} to the fine grid.

For the cascade problem, the following weighted average is used for the interpolation operator I_h^{2h} at the mesh point (i,j),

$$\left[I_h^{2h}(\phi_h)\right]^{(i)} = \frac{1}{4}\left[\phi_h^{(i-1)} + \phi_h^{(i+1)} + 2\phi_h^{i}\right] , \qquad (29)$$

while the linear interpolation is used for the coarse-to-fine interpolation operator I_{2h}^{h} .

Three levels of grids are used in the present work. The corrections to the potential in each grid are computed in the half cycle from fine grid to coarse grid, while the results from the coarser grid are interpolated to the finer grid in the half cycle from coarse grid to fine grid.

In this preliminary study, no attempt has been made to change the method of applying the boundary conditions. They are updated at the end of the smoothing operations. This turns out to be one of the reasons that the preliminary computation does not converge. Each time after the potential on the boundary is updated using the boundary condition, high-frequency error components are reintroduced. They are interpolated into the coarse grid as if they were the low-frequency components. It was pointed out by Jameson and Steinhoff (1981) that the introduction of the relaxing boundary conditions causes the difficulty in applying the multigrid technique in the transonic flow problem. A special treatment of the boundary condition together with a special formula in defining the residue near the boundary is required for the solution to converge. These are some of the focal points for future research.

There are other sources of difficulty in the cascade problem. The mesh system used in the present study has only two upstream boundary cells. As the multigrid cycle goes to the coarser grid, an interior grid point such as A in Figure 4 becomes a boundary point in the coarse grid. Since the freestream conditions are applied in the boundary cells, the boundary points are governed by different operators than the interior points. This violates the assumption that the same mesh point is governed by the same type of operator in

both the coarse and the fine grids. One possible solution to the problem is to modify the mesh system so that at least eight cells are located on the upstream boundary.

In principle, there seems to be no reason why the multigrid technique should not work in the computation of transonic flow past a cascade. There is certainly some research needed in applying the boundary condition correctly in the multigrid computations.

6. Recommendations for the Development of a Three-Dimensional Code

From the present investigation, some insight can be obtained in the extension of the method to three dimensions.

All mesh generation schemes now in use for cascades are based on a conformal transformation of one form or another. If the mesh lines wrap around the leading edge, as O-type and C-type meshes do, then the orthogonality of the conformal transformation results in a mesh system which extends upstream a distance on the order of the pitch distance. From the two-dimensional computations, it seems that the flow around the blade is quite accurately predicted for a pitch-to-chord ratio as low as 1. However, if the flow in a long hub and/or a long shroud ahead of the blade is to be included in the computation, some other mesh system must be patched upstream.

To assemble a series of two-dimensional cascade meshes to form a three-dimensional mesh system, several additional constraints must be satisfied. First of all, the mesh lines leading from the upstream boundary to the blade surface on each spanwise two-dimensional mesh must be connected so that the three-dimensional upstream boundary can be clearly defined. Because of the periodic mesh constraint, the index of this line is always the midpoint in the wraparound direction. Furthermore, to form a clear-cut trailing edge definition, the trailing-edge indices (ITE1 and ITE2) must be maintained for all spanwise stations. To accomplish this, a stretching transformation in the wraparound direction is required. This stretching transformation must apply to all pitch-stagger angle combinations in the realistic range. For a high stagger angle and a large pitch distance, the stretching transformation causes most of the points to cluster on the upper surface of the blade and leaves very few points on the lower surface. This is not a completely satisfactory mesh. However, for the application to turbomachinery, the present mesh generation scheme is probably applicable to all practical ranges of pitch-stagger angle combinations. This expectation needs to be qualified by further investigation.

Currently, research in the application of the so-called H-type mesh to the potential flow calculation is underway (Jou 1980). The H-type grid is essentially a streamline-potential line type of grid which has a transformation singularity. If the development is successful, it may have a profound effect on the development of a three-dimensional code around a rotor.

As to the solution algorithm, the following recommendation is given. The artificial density formulation shows a great deal more tolerance to the grid irregularity as compared to the artificial viscosity. Although the electrostatic mesh generation scheme is expected to give a smooth mesh, some irregularity may arise when the mesh spacing becomes extremely dense, like near the leading edge. A three-dimensional code based on the artificial density formulation is preferred over that using artificial viscosity.

References

Adamczyk, John (1980) "An Electrostatic Analog for Generating Cascade Grids," in Numerical Grid Generation Techniques, NASA Conference Publication 2166, pp. 129-142; also private communications.

Arlinger, B. (1980) "Transonic Flow over Bodies of Revolution," Seventh International Conferences on Numerical Methods in Fluid Dynamics (Preprint), pp. 147-148.

Caughey, D. A., and Jameson, A. (1979) "Progress in Finite Volume Calculations for Wing-Fuselage Combinations," AIAA Paper No. 79-1513R.

Deconinck, H., and Hirsch, C. (1980) "Transonic Flow Calculations with Higher Order Finite Elements," Seventh International Conferences on Numerical Methods in Fluid Dynamics (Preprint), pp. 143-144.

Dulikravich, D. S. (1979) "Numerical Calculation of Inviscid Transonic Flow Through Rotors and Fans," Ph.D. Dissertation, Cornell University, January 1979.

Hafez, M. M. (1979) Unpublished Results Presented at FFA Meeting, Stockholm, September.

Hafez, M. M., Murman, E. M., and South, J. C. (1978) "Artificial Compressibility Methods for Numerical Solution of Transonic Full Potential Equation," AIAA Paper No. 78-1148.

Jameson, A. (1974) "Iterative Solution of Transonic Flows over Airfoils and Wings, Including Flows at Mach 1," Comm. Pure. Appl. Math., Vol. 27.

Jameson, A. (1979) "Acceleration of Transonic Potential Flow Calculations on Arbitrary Meshes by the Multiple Grid Method," AIAA Paper No. 79-1458.

Jameson, A., and Caughey, D. A. (1977) "A Finite Volume Method for Transonic Potential Flow Calculations," AIAA Paper No. 77-635.

Jameson, A., and Steinhoff, J. (1981) Private communications.

Jou, Wen-Huei (1979) "Numerical Solution of Transonic Potential Flow in Turbomachinery," Flow Research Proposal No. 8021, Submitted to NASA Lewis Research Center, October.

Jou, Wen-Huei (1980) "Singularity Embedding Method for Transonic Computations Using Grids with Singularity," Flow Research Proposal No. 8124.

Jupp, J. A. (1980) "Interference Aspects of the A310 High Speed Wing Configuration," Subsonic/Transonic Configuration Aerodynamics, AGARD Conference Proceedings No. 285, pp. 11-1 to 11-16.

Mercer, J. E., and Murman, E. M. (1980) "Application of Transonic Potential Calculations to Aircraft and Wind Tunnel Configurations," AGARD Conference on Subsonic/Transonic Configuration Aerodynamics, May 5-7.

South, J. C., and Brandt, A. (1977) "Application of a Multi-Level Grid Method to Transonic Flow Calculations," in Transonic Flow Problems in Turbomachinery, Washington, D. C., Hemisphere Publishing, pp. 180-207.